A Multi-Mirror Solution for the Deflection of Dangerous NEOS

Massimiliano Vasile

Department of Aerospace Engineering, University of Glasgow, James Watt South Building, Glasgow, G12 8QQ, UK. m.vasile@aero.gla.ac.uk

Abstract

This paper presents some recent results on the deflection of potentially dangerous Near Earth Objects. A particular deflection technique, employing a swarm of mirrors focusing the light of the Sun on the surface of the asteroid, is described. The swarm has to fly in formation with the asteroid, or hover in close proximity. The paper describes two different designs for the mirrors, and different options to place the spacecraft in the vicinity of the asteroid. In particular the paper shows a number of periodic formation orbits. As an alternative, results are shown by placing the spacecraft at fixed points in close proximity to the asteroid, where the solar pressure and the gravity attraction balance each other.

Key words: asteroid deflection, artificial equilibrium points, formation flying, multiobjective optimization
PACS: 96.30.Ys, 02.60.Cb, 02.60.Pn, 95.10.C

1 Introduction

Since the discovery of the asteroid Apophis in December 2004, there has been a revived interest in techniques to deflect asteroids. From the initial observations, Apophis is expected to have a close encounter with the Earth in 2029. During that event Apophis could pass through a gravitational keyhole, a precise region in space no more than about 400 meters across, which would set up a future impact on 13 April 2036. Among the approaches proposed to deflect the trajectory of an asteroid, there are some that consider the generation of a thrust by ablating some surface material. Surface ablation approaches have been proposed in the past using several techniques such as lasers or nuclear explosives. One method in particular conceptualized directing solar energy using mirrors onto a small area on the surface of the asteroid. The idea initially

appeared on the journal *Space Policy*[4] and was later compared to other deflection methods by Melosh et al. [8]. The heat produced by the concentrated solar light is used to sublimate the surface matter creating narrow but expanding jets of gas and debris that produce a low continuous thrust. This low thrust would eventually alter the orbit of the NEO by producing a change in velocity.

In a previous studies by the author [10,11], the sublimation technique was compared against other deflection methods and resulted to be among the most effective methods. However, the use of a single mirror would imply the deployment and control of a significantly large structure in space and presents a number of difficulties from several points of view, recently pointed out by Kahle et al.[3].

While some difficulties are related to the control of the mirror in proximity of the asteroid, others are related to the positioning of the mirrors in order to avoid any impingement with the plume of gas and debris leaving the asteroid, and at the same time maintain the required power density on its surface. A possible solution would be to use a swarm of mirrors that would focus the light of the Sun on the same spot on the surface of the asteroid. The launch, deployment and control of each spacecraft would be more practical than for a single mirror, and the system would be intrinsically redundant and scalable (for a bigger asteroid, we would need to add more spacecraft but the design of each spacecraft would not require any modification or further development).

In a recent study [5], it was demonstrated how a significant deviation of the asteroid Apophis could be achieved with a relatively small number of satellites (20 to 40) each carrying a relatively small primary mirror (between 10 and 40 meters in diameter). Fig. 1 shows a comparison of the required minimum diameter of the aperture of the primary parabolic mirror versus the duration of the thrust. The comparisons were done for different swarm sizes ranging from a single spacecraft (for a baseline comparison) up to 5000. For each swarm size, the diameter of the illuminated spot size on the surface of the asteroid was set to $0.5m$ or $1.5m$. The difference can be seen as the duration of the thrust increases; the lower branch corresponds to the $0.5m$ spot size, and the upper branch, the $1.5m$. This is expected as the higher the power density, the smaller the spot size (or a higher concentration ratio for the same incoming solar power). The deviation distance was nominally fixed equal to the Earth-Moon distance at the Minimum Orbital Interception Distance (MOID) from the Earth.

However, placing the mirrors in proximity of the asteroid was still an open issue. In particular the analysis of the orbital maintenance of the mirrors was still missing. In this paper, the multi-mirror option is presented together with an analysis of the positioning of the mirrors in the vicinity of the asteroid. A

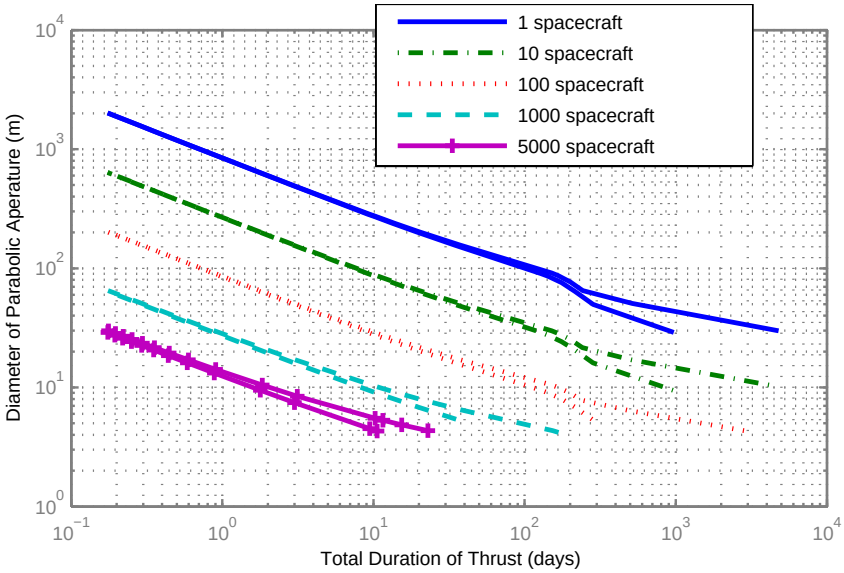

Fig. 1. Diameter of the mirror vs total duration of the deviation action for a variable number of spacecraft for a fixed deviation of the orbit of Apophis of 384403 km (Earth-Moon distance) at the MOID.

model for two different configurations – a novel single and dual-mirror configuration – will be presented. Apophis is used as case study because of the relatively high threat posed by this particular asteroid.

The first section of the paper will describe the two mirror configurations and the derivation of the force due to the solar pressure acting on the spacecraft. The second section will present a family of formation orbits that can be used to place and control the mirrors. The third section will present an alternative method to place and control the mirrors at artificial equilibrium points (AEPs) in proximity of the asteroid.

2 Mirror Design

The design of the device that is focusing the light of the Sun on the surface of the asteroid is a critical aspect of this deflection method. The device has to be able to concentrate a minimum power density at all times (see Sanchez et al. [11] for further details). Therefore, it is required to have the capability to steer the beam of light to hit any part of the asteroid and to control the concentration factor (or amount of light that is focused on a particular spot).

Here we propose two different configurations for the focusing device: a parabolic symmetric primary mirror with collimating lens and secondary directional mirror (Fig. 2a), and an asymmetric focusing mirror with collimating lens and no directional mirror (Fig. 2b). In the former case the primary mirror always

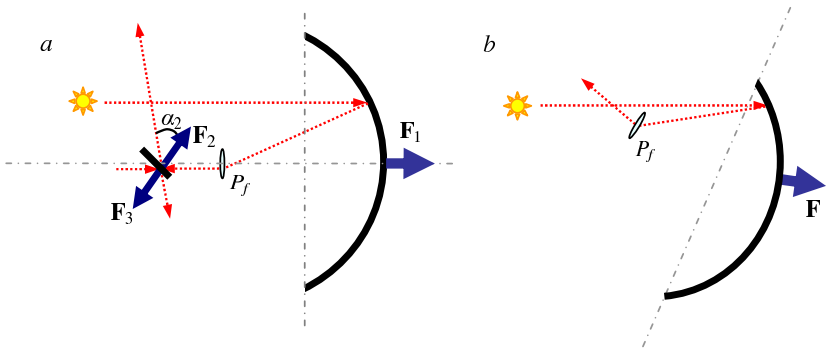

Fig. 2. Dual-mirror (left) and single mirror (right) configurations.

points toward the Sun. The lens(es) produces a collimated beam of light that reflects on the secondary mirror and is projected onto the surface of the asteroid. In the latter case the primary mirror should be properly oriented based on the Sun vector. The configuration in Fig. 2b can be easily modified by removing the lens and focusing the light directly on the surface of the asteroid. If the light is focused directly on the surface of the asteroid, the focal point has to be moved away from the mirror and the mirror will result in being almost flat.

Since the mirrors are moving with respect to the asteroid, we introduce a local rotating reference frame centered in the barycenter of the asteroid (Hill's reference frame in Fig. 3). In this reference frame, the x axis is aligned with the Sun-asteroid vector, the y axis is the direction of motion and the z axis is perpendicular to the asteroid orbital plane in the direction of the orbital angular momentum.

2.1 Single Mirror Configuration

The single mirror configuration is composed of an asymmetric adaptive primary mirror and of a collimating lens (or set of lenses). The shape of the primary mirror is assumed to be adaptable such that the focal point can be moved in order to steer the beam in the desired direction.

In order to define the shape of the mirror and its attitude with respect to the Sun we introduce the mirror reference frame in Fig. 4, with coordinated axes x_M, y_M, z_M. The mirror reference frame is tilted by an angle β with respect to the Hill's reference frame and is centered in the center of mass of the mirror assembly. Note that in the following analysis we assume that the spacecraft is a point mass and therefore the position of its barycenter does not change for any variation of the shape of the mirror.

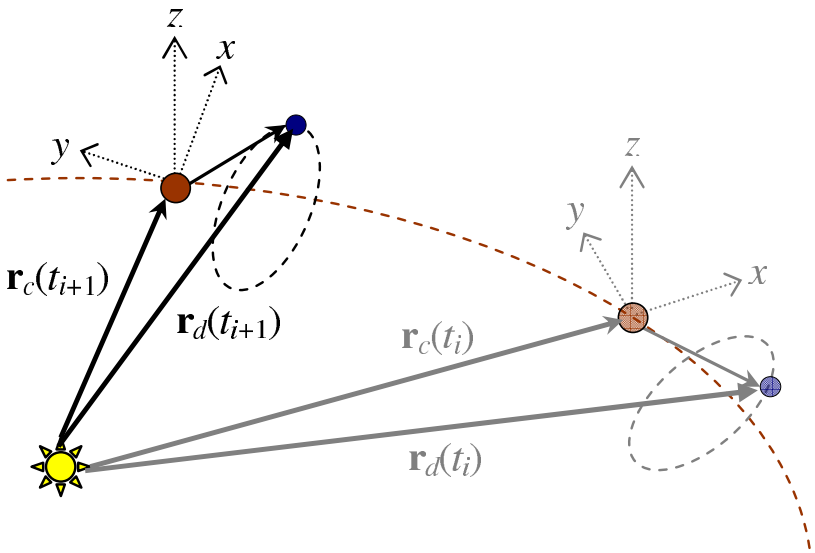

Fig. 3. Hill's rotating reference frame in the radial x, transversal y and normal z directions.

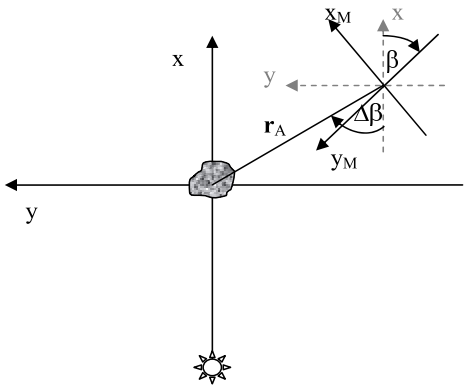

Fig. 4. Definition of the mirror reference frame with respect to the Hill's rotating reference frame.

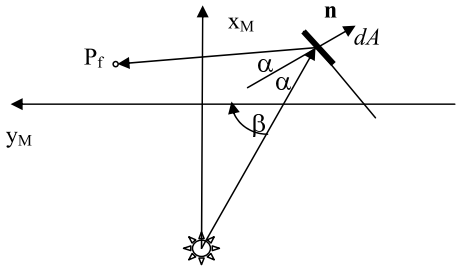

Fig. 5. Geometry for mirror design.

Now, given the position of the focal point P_f in the mirror reference frame and the position of a mirror element with infinitesimal area dA, the law of

reflection (assuming a perfect reflection) gives us (see Fig. 5):

$$\frac{dx_M}{dy_M} = \tan\left[\beta - \pi/2 - \alpha\left(x_M, y_M, x_f, y_f, \beta\right)\right] \tag{1}$$

where $[x_f, y_f]$ is the position of the focal point P_f, β is the Sun aspect angle with respect to the reference frame of the mirror assembly and α is the reflection angle. Note that the angle β also represents the attitude angle of the mirror reference frame with respect to the Hill's reference frame and therefore will be referred to as the attitude angle of the mirror in the following. By integrating Eq. 1 with initial conditions y_{M_0} and x_{M_0}, we can get the shape of each section of the mirror in the x_M-y_M plane given the position of P_f and the direction of the incoming Sun rays. In the following, we will define the focal distance as $f_p = x_f - x_{M_0}$. The mirror is then considered to be symmetric with respect to the x_M-y_M plane such that each section of the mirror parallel to the x_M-z_M plane is a parabola with focus P_f.

Once the shape and orientation of the mirror are defined, the total force acting on the mirror assembly can be computed by integrating the following expression over the surface of the mirror A:

$$d\mathbf{F} = 2\eta_M P cos^2\alpha \mathbf{n} dA \tag{2}$$

$$\mathbf{F}_{SM} = 2\eta_M P \int_A cos^2\alpha \mathbf{n} dA \tag{3}$$

where the solar pressure at $1AU$ is $P_0 = 4.563 \cdot 10^{-6}\ N/m^2$, P is the solar pressure at a distance r_d from the Sun $P = P_0(r_{1AU}/r_d)^2$, r_{1AU} is one astronomical unit and η_M is the efficiency of the mirror (assumed to be 1.0).

2.2 Dual-mirror Configuration

For the dual-mirror configuration, three forces have to be taken into account: $\mathbf{F}_1 = \eta_{pri} A_{pri} P\left(\mathbf{r}_d/r_d\right)$ is the force due to the solar pressure acting onto the primary mirror, $\mathbf{F}_2$ is the force due to the solar pressure acting onto the secondary mirror and $\mathbf{F}_3$ is the force due to the reflected light from the primary mirror onto the secondary mirror.

The primary mirror in this configuration is assumed to be parabolic and always pointing toward the Sun, while the secondary mirror is flat. Due to the concentration factor, the power density of the reflected light is higher than the one of the direct light, therefore, though the surface of the secondary mirror

is smaller than the one of the primary, the reflected solar light exerts a force on the secondary mirror which is:

$$\mathbf{F}_3 = -\left(2\eta_{sec} cos^2\alpha_2\right) \eta_{pri} A_{pri} P \, \mathbf{n}_2 \tag{4}$$

while $\mathbf{F}_2$ is simply:

$$\mathbf{F}_2 = \left(2\eta_{sec} cos^2\alpha_2\right) A_{sec} P \, \mathbf{n}_2 \tag{5}$$

Both forces are acting in the direction normal to the secondary mirror surface $\mathbf{n}_2$.

The total force acting on the mirror assembly (i.e. primary, secondary mirror and lenses) is given by:

$$\mathbf{F}_{DM} = \mathbf{F}_1 + \mathbf{F}_2 + \mathbf{F}_3 \tag{6}$$

expressed as a vector in the local Hill's reference frame.

3 Funnel Formation Orbits

One option is to consider the asteroid as a point mass and the spacecraft flying in formation with it, the asteroid being the chief or target and the spacecraft the chasers. As a first approximation, the gravity field of the asteroid is considered to have negligible influence on the motion of the spacecraft. This situation corresponds to the spacecraft flying outside the sphere of influence of the asteroid or compensating for its gravity attraction with an active control. Furthermore, it is assumed that no other forces are acting on the spacecraft apart from the gravity attraction of the Sun. The position vector of the spacecraft is therefore given by[12]:

$$\begin{aligned}
&x(\theta) = \tfrac{r_c}{a}\delta a - a\cos\theta\delta e + \tfrac{ae\sin\theta}{\eta}\delta M \\
&y(\theta) = \tfrac{r_c\sin\theta}{\eta^3}(2 + e\cos\theta)\delta e + r_c\cos i\tfrac{r_c}{\eta^3}(1 + e\cos\theta)^2\delta\Omega + \\
&r_c\delta\omega + \tfrac{r_c}{\eta^3}(1 + e\cos\theta)^2\delta M \\
&z(\theta) = r_c\sin\theta^*\delta i - r_c\cos\theta^*\sin i\delta\Omega
\end{aligned} \tag{7}$$

where $p = [a, e, i, \omega, \Omega, M]^T$ are the orbital parameters of the asteroid, $\delta p = [\delta a, \delta e, \delta i, \delta\omega, \delta\Omega, \delta M]^T$ their variation, $\eta = \sqrt{1 - e^2}$, r_c is the modulus of the inertial orbital radius of the asteroid, θ is the true anomaly, $\theta^* = \theta + \omega$ is the

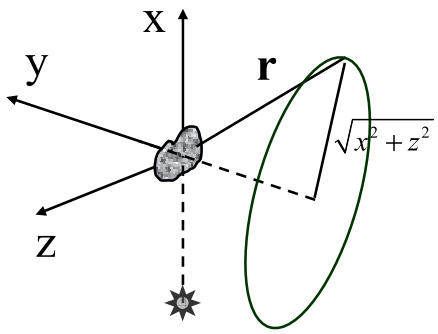

Fig. 6. Geometry for the design of funnel orbits.

true latitude, $h = \eta\sqrt{a\mu_S}$ is the orbital momentum, μ_S is the gravity constant of the Sun and x, y and z are the local cartesian Hill's frame coordinates.

The motion described by Eqs. 7 is governed by the dynamic equations[12]:

$$\begin{aligned}
\ddot{x} &= 2\dot{\theta}(\dot{y} - y\tfrac{\dot{r}_c}{r_c}) + x\dot{\theta}^2 + \tfrac{\mu_S}{r_c^2} - \tfrac{\mu_S}{r_d^3}(r_c + x) \\
\ddot{y} &= -2\dot{\theta}(\dot{x} - x\tfrac{\dot{r}_c}{r_c}) + y\dot{\theta}^2 - \tfrac{\mu_S}{r_d^3}y \\
\ddot{z} &= -\tfrac{\mu_S}{r_d^3}z
\end{aligned} \tag{8}$$

We want to maintain a periodic motion of the mirrors in the proximity of the asteroid therefore we impose the condition for periodicity $\delta a = 0$ which guarantees that δM is constant.

Given that all the mirrors will have to focus the light onto the same spot, the pointing requirements should be minimized, which implies a close proximity to the asteroid. On the other hand, it is desirable to limit the gravitational perturbations from the asteroid and therefore the satellites should fly outside a limit sphere. In addition, the satellites should avoid impingement with the exhaust gases caused by the sublimation of the asteroid material.

If we assume that the optimal thrust direction that maximizes the deviation is along the unperturbed velocity vector of the asteroid [14,1] then the exhaust gasses will flow along the y axis of the local Hill's reference frame. The problem can be formulated in mathematical terms as follows (see Fig. 6):

$$\min_{\delta\mathbf{p}\in D} \min_{\theta} f_1 = r \tag{9}$$

$$\min_{\delta\mathbf{p}\in D} \min_{\theta} f_2 = -\sqrt{x^2 + z^2} \tag{10}$$

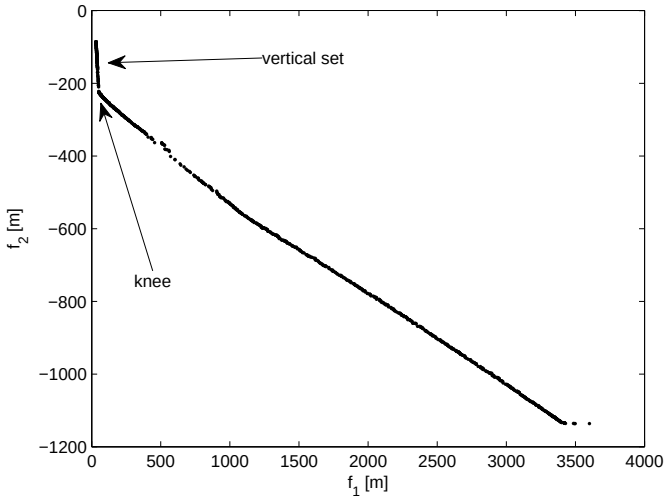

Fig. 7. Pareto front for the funnel orbits problem.

subject to the constraint:

$$C = \min_{\theta}(r(\theta) - r_{sph}) > 0 \tag{11}$$

where and r_{sph} is a limit sphere and D is the search space for the solution vector $\delta\mathbf{p}$ and $r = \|\mathbf{r}\|$ is the modulus of the position vector of the mirror with respect to the asteroid $\mathbf{r} = [x, y, z]^T$. The problem in Eqs. 9, 10 and 11 was solved with a hybrid stochastic-deterministic approach based on a multiagent search technique combined with a decomposition of the search space [6,13]. Fig. 7 shows the resulting Pareto optimal solutions to Eq. 9 for $r_{sph} = 2.3\ km$, which is a limit imposed to avoid the effects of the inhomogeneous gravity field of the asteroid.

Fig. 8 is showing the set of Pareto optimal solutions in the parameter space. As can be seen, the solutions are symmetrically distributed about the value 0 of the δ parameters. It is interesting to note that for the same value of $\delta\omega$ or $\delta\Omega$, there are multiple values for f_1 and f_2. This suggests the existence of multiple families of formation orbits with different characteristics with respect to the criteria f_1 and f_2. The whole set of Pareto optimal orbits are represented in Fig. 9. They form two *funnels* growing in diameter as the orbits move away from the asteroid. The Pareto front in Fig. 7 presents an almost vertical set of points and a 'knee' where the front changes slope. The orbits belonging to the vertical set are represented in Fig. 10 (left graph). In the same figure (right graph), we also plotted some particular solutions with a higher value of f_1 and f_2. These solutions form four families of symmetric orbits. The existence of these solutions suggests that the problem may present four complete funnels, and not just two as in Fig. 9, where for the other two funnels only few orbits are represented.

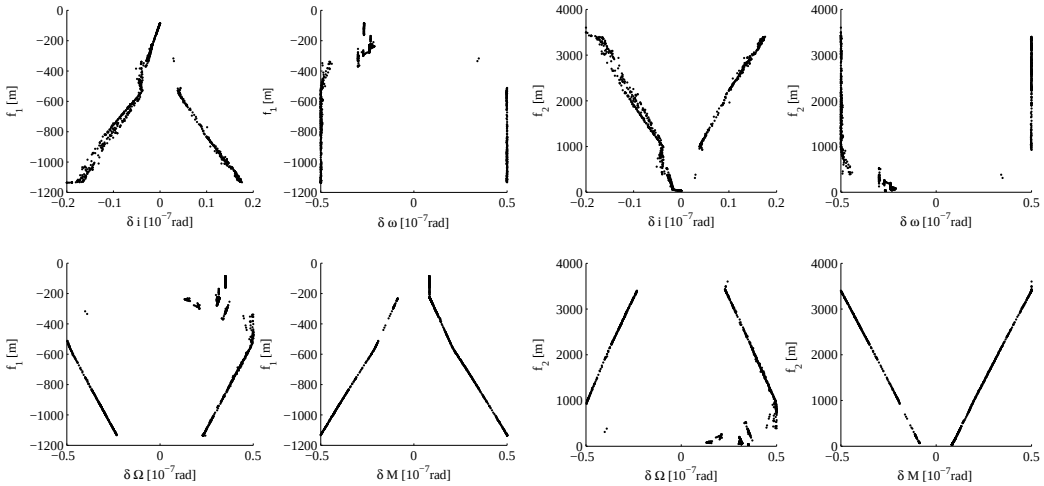

Fig. 8. δ parameter for Pareto optimal solutions, all values are scaled by 1e-7.

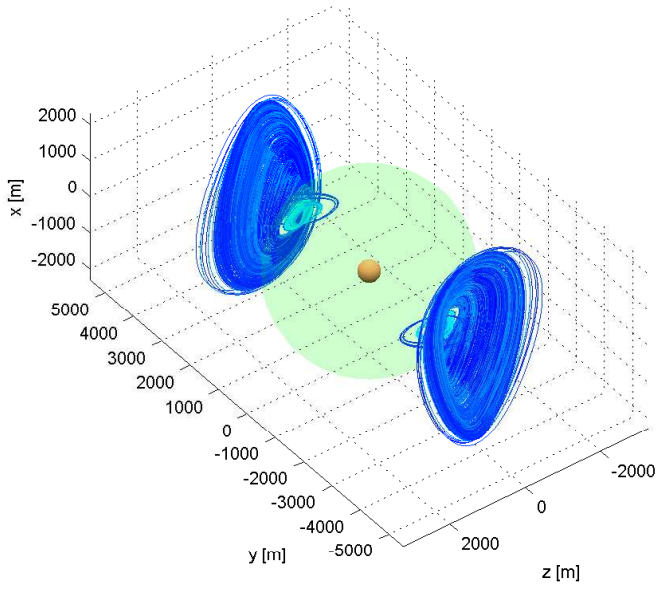

Fig. 9. Funnel configuration for the solutions of Eq. 9 with $r_{sph} = 2300\ m$.

A similar configuration can be also obtained for a limit sphere of 45 km which corresponds to the distance at which the gravity of the asteroid becomes irrelevant. In this case, though, the pointing accuracy would be one order of magnitude higher.

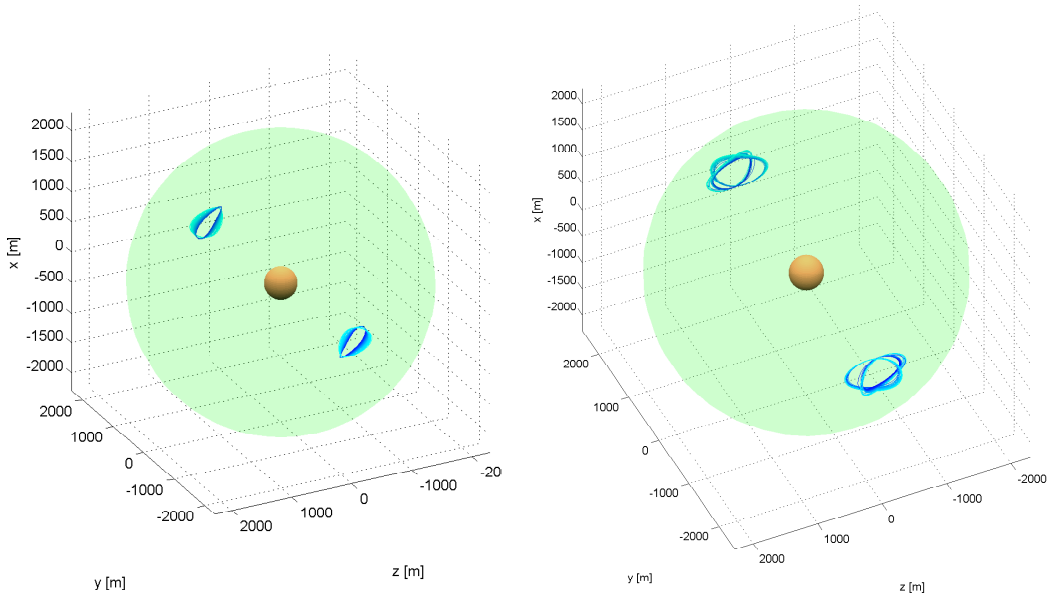

Fig. 10. Funnel configuration for the solutions of Eq. 9 with $r_{sph} = 2300\ m$: left figure represents the solutions in the vertical part of the Pareto set before the knee, right figure represents two families of symmetric orbits for each funnel.

3.1 Orbit Maintenance

Funnel formation orbits were designed assuming no solar pressure and no gravity attraction from the asteroid. In order to consider the gravity attraction from the asteroid negligible, as mentioned before, the mirror should be placed outside the sphere of influence of the NEO, with a consequent stringent requirement on the pointing capabilities of the mirror. Furthermore, although at that distance the gravity of the asteroid becomes negligible, the solar pressure still plays an important role in the dynamics of the spacecraft. Another option is to compensate for the gravity attraction and for the solar pressure. If this strategy is adopted a thrust has to be generated in the opposite direction of the resultant of the two forces.

Eqs. 8 assume that the asteroid is not a gravitational body and that there is no other force than the gravity attraction of the Sun. If the contribution of the gravity field of the asteroid and of the solar pressure are taken into account, Eqs. 8 have to be rewritten in the following form:

$$\begin{aligned}
\ddot{x} &= 2\dot{\theta}(\dot{y} - y\tfrac{\dot{r}_c}{r_c}) + x\dot{\theta}^2 + \tfrac{\mu_S}{r_c^2} - \tfrac{\mu_S}{r_d^3}(r_c + x) - \tfrac{\mu_A}{r^3}x + \tfrac{\hat{s}_x(x,y,z)}{m} + \tfrac{u_x}{m} \\
\ddot{y} &= -2\dot{\theta}(\dot{x} - x\tfrac{\dot{r}_c}{r_c}) + y\dot{\theta}^2 - \tfrac{\mu_S}{r_d^3}y - \tfrac{\mu_A}{r^3}y + \tfrac{\hat{s}_y(x,y,z)}{m} + \tfrac{u_y}{m} \\
\ddot{z} &= -\tfrac{\mu_S}{r_d^3}z - \tfrac{\mu_A}{r^3}z + \tfrac{\hat{s}_z(x,y,z)}{m} + \tfrac{u_z}{m}
\end{aligned} \tag{12}$$

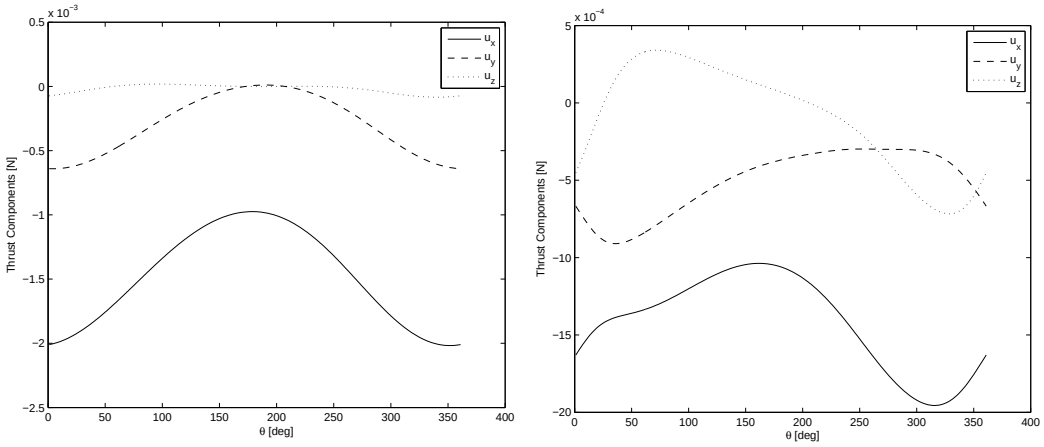

Fig. 11. Funnel orbits: (left) the controls for a Pareto solution at the knee of the Pareto front; (right) the controls for the solution farthest away from the asteroid.

where μ_A is the gravity constant of the asteroid, $\mathbf{u} = [u_x, u_y, u_z]^T$ is the control force, m is the mass of the spacecraft, and the contribution of the solar pressure $\mathbf{F}_{SM} = [\hat{s}_x, \hat{s}_y, \hat{s}_z]^T$ is derived from Eq. 6

We can now estimate the required control capabilities by plugging the position and velocity time history for the funnel orbits into the equations of motion and solving for the control required to compensate for solar pressure and gravity attraction of the asteroid. We assume here an initial mass of the spacecraft $m = 2000\ kg$ and a surface area of the primary mirror $A_{pri} = 196\ m^2$ with a secondary mirror of $0.5\ m$ in diameter.

Fig. 11 represents the three components of the control thrust for the formation orbit at the knee of the Pareto front (left graph) together with the control thrust for the formation orbit furthest away from the asteroid (right graph). It is interesting to note that the magnitude of the control for the two orbits is quite similar. This suggests, as expected, that the controls are mainly compensating for the solar pressure, with the gravity attraction of the asteroid being less significant.

4 Artificial Equilibrium Points for a Solar Concentrator

If solar pressure and the gravity field of the asteroid are taken into account then the mirrors can be designed so that the two forces are in equilibrium, with the spacecraft hovering at a fixed location (and distance) from the asteroid. Note that unlike the problem of finding AEPs for a flat reflector[7], here we analyze the case of a curved reflector with pointing constraints.

Considering that the mirror has to constantly reflect the light onto the surface

of the asteroid (pointing constraint), if the mirror was flat the only possible equilibrium configuration would be with the asteroid-mirror direction aligned with the spacecraft-Sun direction. If the mirror is not flat, instead, then we can look for possible position vectors $\mathbf{r}$, solar aspect angles β and focal distances f_p such that the vector $\mathbf{F}_{SM} = [s_x, s_y, s_z]^T$ is aligned with the asteroid-mirror direction and:

$$\begin{aligned} &-2\dot{\theta}y\tfrac{\dot{r}_c}{r_c} + x\dot{\theta}^2 + \tfrac{\mu_S}{r_c^2} - \tfrac{\mu_S}{r_d^3}(r_c + x) - \tfrac{\mu_A}{r^3}x + \tfrac{s_x(x,y,z,\beta,f_p)}{m} = 0 \\ &2\dot{\theta}x\tfrac{\dot{r}_c}{r_c} + y\dot{\theta}^2 - \tfrac{\mu_S}{r_d^3}y - \tfrac{\mu_A}{r^3}y + \tfrac{s_y(x,y,z,\beta,f_p)}{m} = 0 \\ &-\tfrac{\mu_S}{r_d^3}z - \tfrac{\mu_A}{r^3}z + \tfrac{s_z(x,y,z,\beta,f_p)}{m} = 0 \end{aligned} \tag{13}$$

Note that, the force due to solar pressure is obtained from Eq. 2. In the following, we will consider only the planar case with $z = 0$, since in this case the third equation in Eq. 13 is satisfied.

Figs. 13 represent the misalignment of the force vector due to the solar pressure with respect to the spacecraft-asteroid direction for two different focal lengths. In the figures L is the length of the projection of the mirror onto the y_M axis of the mirror reference frame. The angle β, as before, is the direction of the light impacting on the mirror while $\Delta\beta$ is the angle between the incoming sunlight and the direction of the focal point of the mirror (see Fig.4). The direction of the focal point identifies the pointing direction. We consider only one quadrant of the Hill's frame with positive x and negative y. For positive x and positive y the solutions are symmetric; there are no solutions in the other two quadrants.

As it can be seen for $\beta = \pi/2$, the only equilibrium solutions are along the Sun-asteroid direction. However, in this case the mirror would be in shadow and therefore no equilibrium points can exist along that direction. For higher values of β, equilibrium points can exist at higher angular distances from the radial direction. For example, for $\beta = 139\ deg$ the mirror can be placed at $\mathbf{r} = [1.3699, 0.48225, 0]^T\ km$, which is about 20 deg from the radial direction (Fig. 12 shows the level of acceleration acting on the spacecraft).

This artificial equilibrium point offers a good location for projecting the light of the Sun on the side of the asteroid along the y direction, and away from the plume of gases. If we assume that the lens produces a collimated light beam with negligible divergence, and that the beam is projected at the intersection of the surface of the asteroid with the y-axis, then we can compute where the two extreme points of the beam intersect the surface of the asteroid. From this intersection, we can compute the spot size given the beam size and the elevation over the y-axis. As can be seen in Fig. 15, for a beam size between 0.5 and 1 m in diameter, the increase in spot size due to an elevation of 70

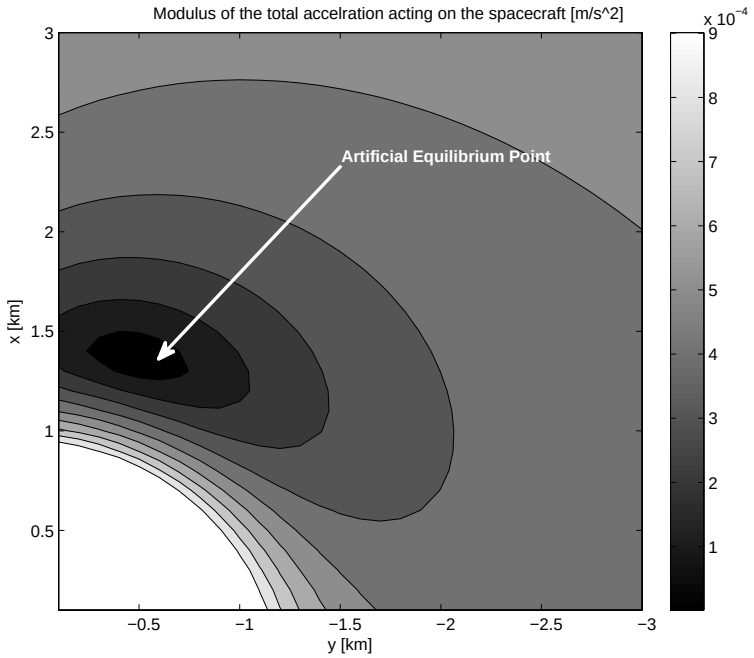

Fig. 12. Example of AEP at 20 *deg* from the radial direction.

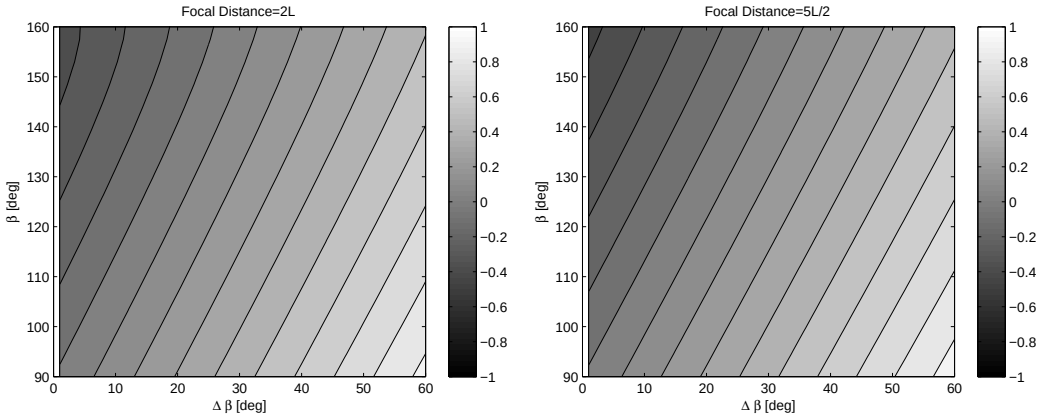

Fig. 13. Misalignment between the position vector **r** and the direction of resultant force due to solar pressure: (left) the misalignment for a focal distance equal to $2L$; (right) the misalignment for a focal distance equal to $2.5L$.

degrees along the y-axis and 20 degrees from the radial x-axis, is still limited.

4.1 Orbit Maintenance

Solar pressure depends on the distance from the Sun, therefore, if the size of the mirror is constant, as the asteroid moves around the Sun the force acting to the spacecraft changes with the true anomaly θ. As a consequence, the

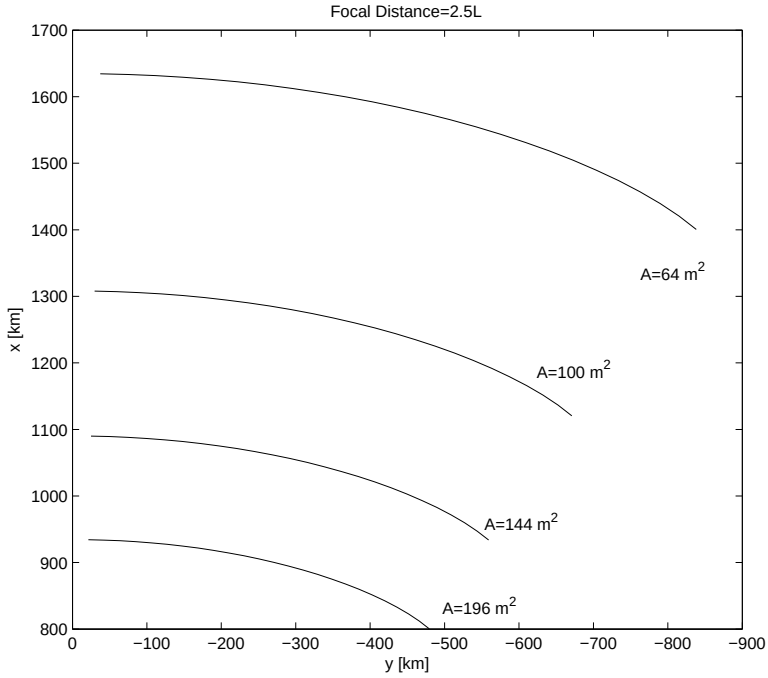

Fig. 14. Artificial Equilibrium points for different mirror sizes.

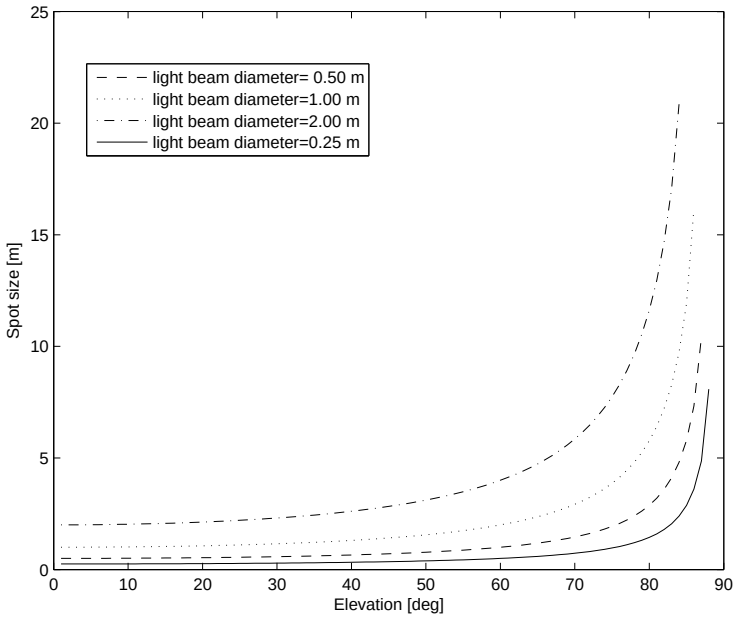

Fig. 15. Increase in the spot size as a function of the elevation over the y axis.

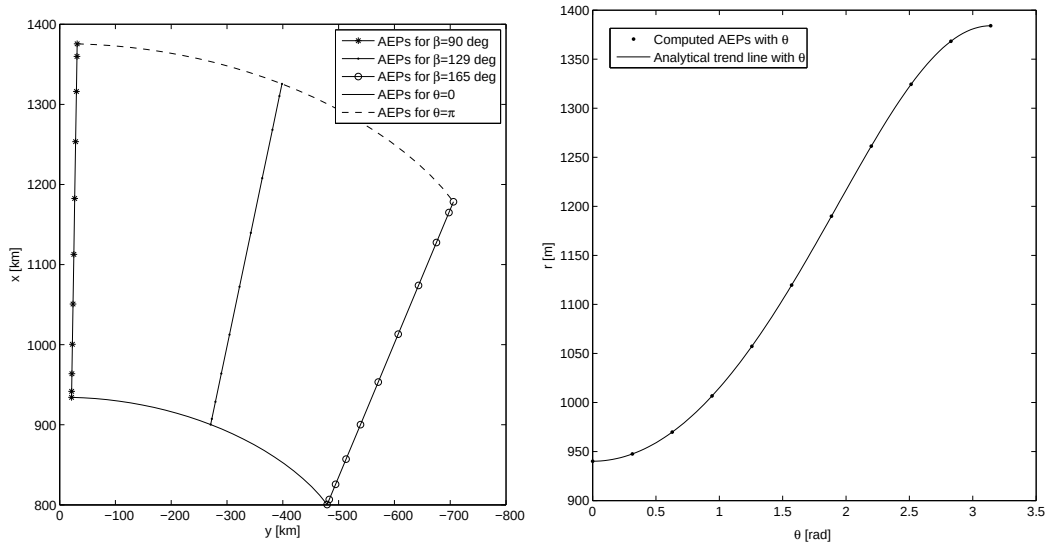

Fig. 16. Variation of the equilibrium points with the true anomaly for $A = 196\ m^2$.

position of the equilibrium points changes with time unless the orbit of the asteroid is circular.

Fig. 16 shows, for different attitudes of the mirror (left plot), the position of the equilibrium points over a full orbit of the asteroid Apophis. Fig. 16 also shows (right plot) the variation of the position of the AEP for a particular attitude of the mirror, over half an orbit. The black dots represent the computed position of the equilibrium points for an angle $\beta = 129\ deg$ while the continuous line is given by the following equations,

$$\begin{aligned} x_{AEP} &= r_{AEP}(\theta_0)\cos(\epsilon)(1 + e\cos(\theta_0))/(1 + e\cos(\theta)) \\ y_{AEP} &= r_{AEP}(\theta_0)\sin(\epsilon)(1 + e\cos(\theta_0))/(1 + e\cos(\theta)) \end{aligned} \tag{14}$$

where $\epsilon = \arctan\left[\frac{y_{AEP}(\theta_0)}{x_{AEP}(\theta_0)}\right]$ is the angular position of the AEP for $\theta = \theta_0$. Then, the distance of the AEP from the asteroid varies with the following law:

$$r_{AEP} = r_{AEP}(\theta_0)(1 + e\cos(\theta_0))/(1 + e\cos(\theta)) \tag{15}$$

Since the AEPs are moving, a spacecraft placed at an AEP would move toward the asteroid or away from the asteroid depending on the initial θ. Specifically, for $\theta \in [0, \pi]$ the spacecraft would fall toward the asteroid, while for $\theta \in [\pi, 2\pi]$ the spacecraft would escape along the radial direction.

We can envisage two strategies to maintain the orbital position of the mirror: compensating for solar pressure and gravity attraction with an active control (low-thrust)or letting the spacecraft drift along the radial direction chasing

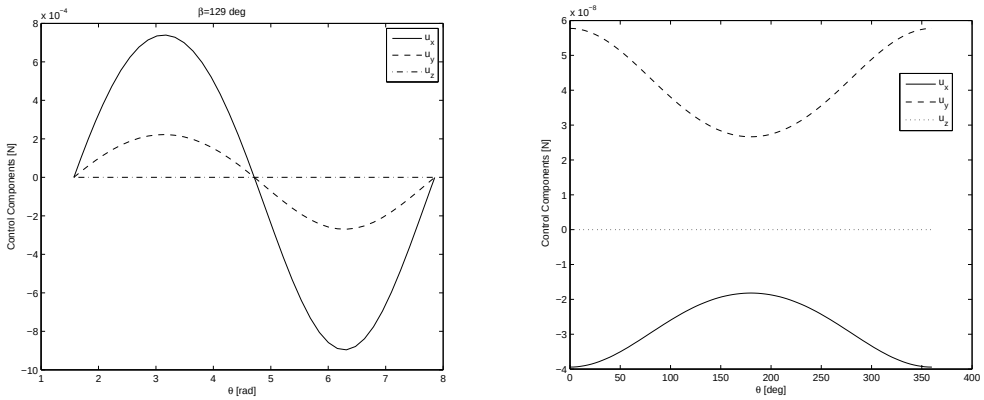

Fig. 17. Control profiles for orbit maintenance for $A = 196\ m^2$.

the position of the equilibrium points.

In order to chase the AEP the spacecraft has to move with the same kinematics, therefore we can impose the following velocity and acceleration:

$$\frac{dx}{dt} = \frac{dr_{AEP}}{dt}\cos(\epsilon) \qquad \frac{dy}{dt} = \frac{dr_{AEP}}{dt}\sin(\epsilon) \tag{16}$$

$$\frac{d^2x}{dt^2} = \frac{d^2r_{AEP}}{dt^2}\cos(\epsilon) \qquad \frac{d^2y}{dt^2} = \frac{d^2r_{AEP}}{dt^2}\sin(\epsilon) \tag{17}$$

with:

$$\frac{dr_{AEP}}{dt} = \frac{r_{AEP}^2 e\sin(\theta)\dot{\theta}}{r_{AEP_0}} \tag{18}$$

$$\frac{d^2r_{AEP}}{dt^2} = \frac{er_{AEP}}{r_{AEP_0}}\left[2\dot{r}_{AEP}\sin(\theta)\dot{\theta} + r_{AEP}\cos(\theta)\dot{\theta}^2 + r_{AEP}\sin(\theta)\ddot{\theta}\right] \tag{19}$$

Eqs. 16 and 17 represent an imposed shape to the motion of the spacecraft. If we then substitute Eqs. 14, 16 and 17 into the dynamic equations and solve for the controls we can get the required thrust components to follow the prescribed kinematics.

In Fig. 17 we present an example of thrust profile for the former strategy (left image) and for the latter strategy (right image).

As it can be seen, the control capability required to maintain a fixed position is greater than the one required to chase the AEP. A possible scenario, therefore, is that the swarm can be distributed around the asteroid at different angles ϵ and the mirrors would move back and forth along the radial directions.

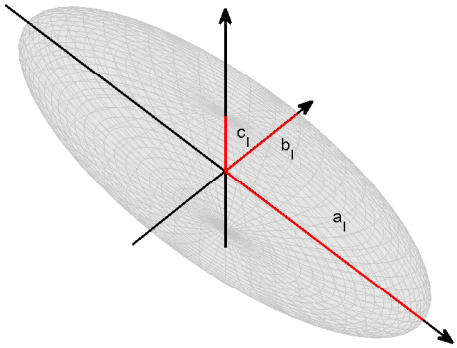

Fig. 18. Geometry of an ellipsoidal asteroid.

4.2 AEPs for a Non-spherical Asteroid

The analysis presented in the previous section is valid for a spherical asteroid with a homogenous gravity field. However asteroids have an irregular shape with a very inhomogeneous gravity field. As done previously by other authors, we can assume that the asteroid is an ellipsoid with semi-axes a_I, b_I and c_I (see Fig. 18). In particular we assume that the semi-axis c_I is aligned with the z axis of the Hill's frame and that the asteroid is rotating around the z axis with angular velocity ω_R. Note that the rotation around z is most likely not the only motion associated to an irregular asteroid. For example, it can be expected that an irregular body is also wobbling but these additional motion components are not considered in the present analysis. Furthermore, during the ablation process the mass of the asteroid changes (see Ref.[11]) as well as its shape. In fact, the strategy considered here and in Sanchez et al. [11] is not to track a fixed spot on the surface of the asteroid but to keep the the direction of the beam substantivally fixed, as the surface of the asteroid moves under the spotlight. The result is to plough the asteroid as the sub-satellite point is moving along its surface. Moreover, in the ideal case, the lenses should generate a perfectly collimated beam, thus no adaptive focusing would be needed when the surface of the asteroid moves away or closer to the mirror. In the real case, instead, it is expected that the position of the lenses can be controlled to improve the focusing of the beam. However, even the change in mass and shape of the asteroid is not considered in the present analysis, as it is minimal over short periods of time, and will be addressed in a future study.

With this assumptions we can express the gravity field of the asteroid as the sum of a spherical field plus a second-degree and second-order field[2,9]:

$$U_{20+22} = \frac{\mu_A}{r^3}[C_{20}(1 - \frac{3}{2}\cos^2\delta) + 3C_{22}cos^2\delta\cos 2\lambda] \tag{20}$$

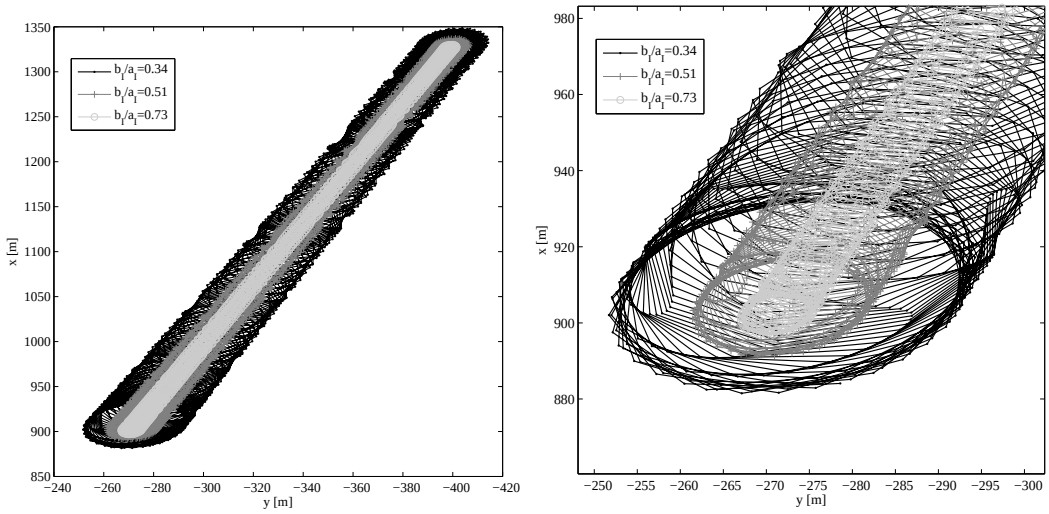

Fig. 19. AEPs for a non spherical asteroid: (left) AEPs for different elongations and for a full revolutions of the asteroid; (right) a close up for few degrees around the perihelion.

where the harmonic coefficients C_{20} and C_{22} can be expressed as a function of the semi-axes:

$$\begin{aligned} C_{20} &= -\tfrac{1}{10}(2c_I^2 - a_I^2 - b_I^2) \\ C_{20} &= \tfrac{1}{20}(a_I^2 - b_I^2) \end{aligned} \tag{21}$$

and the angles δ and λ are defined as:

$$\begin{aligned} \delta &= 0 \\ \lambda &= \arctan(\tfrac{y}{x}) + \omega_R t \end{aligned} \tag{22}$$

Note that as before we are only interested in the in-plane motion and therefore δ is taken equal to 0. The equations for the equilibrium points then become:

$$\begin{aligned} -2\dot{\theta}y\tfrac{\dot{r}_c}{r_c} + x\dot{\theta}^2 + \tfrac{\mu_S}{r_c^2} - \tfrac{\mu_S}{r_d^3}(r_c + x) - \tfrac{\mu_A}{r^3}x + \tfrac{s_x}{m} + \tfrac{\partial U_{20+22}}{\partial x} = 0 \\ 2\dot{\theta}x\tfrac{\dot{r}_c}{r_c} + y\dot{\theta}^2 - \tfrac{\mu_S}{r_d^3}y - \tfrac{\mu_A}{r^3}y + \tfrac{s_y}{m} + \tfrac{\partial U_{20+22}}{\partial y} = 0 \\ -\tfrac{\mu_S}{r_d^3}z - \tfrac{\mu_A}{r^3}z + \tfrac{s_z}{m} + \tfrac{\partial U_{20+22}}{\partial z} = 0 \end{aligned} \tag{23}$$

We assume an angular speed of one revolution every 30 hours as for the astroid Apophis and three different elongations: $b_I/a_I = 0.73$, $b_I/a_I = 0.51$ and $b_I/a_I = 0.34$. Since we are interested only in the in-plane motion, we can set $c_I = b_I$. Fig. 19 shows the position of the AEPs for the three different elongations over one full orbit of the asteroid around the Sun.

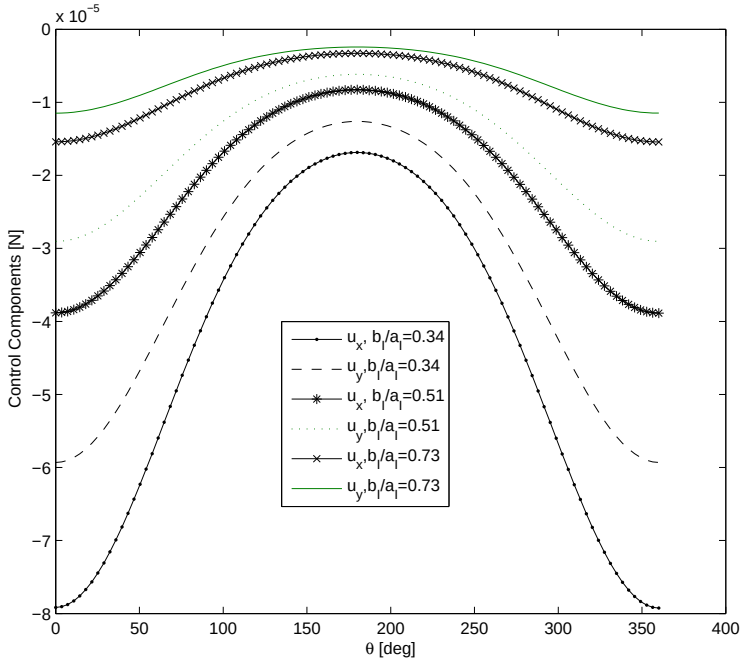

Fig. 20. AEPs station keeping control for a non spherical asteroid.

If now we apply the same control strategy as proposed in the previous section and we force the spacecraft to follow the position of the AEP for a spherical asteroid we get the control profiles represented in Fig. 20.

5 Final Remarks

In this paper we presented an analysis of the proximal motion of a set of mirrors with respect to an asteroid. Two configurations for the mirrors were analyzed and for each one a different strategy for orbit maintenance was considered. In particular, the dual-mirror configuration led to the definition of a particular set of formation orbits composing two symmetric funnels with the principal axis aligned with the y-axis of the Hill's reference frame. These funnel orbits allow the spacecraft to have a very good visibility of the target spot on the surface of the asteroid and at the same time give some room for the plume of gas to flow with minimal impingement. The funnel orbits are located outside a limit sphere, where the gravity field of the asteroid can be considered homogenous. This limit sphere imposes a requirement on the pointing accuracy and on the focusing capabilities of the mirror assembling. A second option considered a single-mirror configuration. For this second option the mirror can be placed at artificial equilibrium points quite inclined over the y-axis of the Hill frame. From this position, the spacecraft sees the target point on the surface of the asteroid from a high elevation angle. However, AEPs can be found such that

the distortion of the spot area due to the elevation angle is limited. For this second option a control strategy was proposed that allows the spacecraft to oscillate in a confined region in the proximity of the asteroid with very low control thrust. Even adding the effect of the gravity field of an elongated body the magnitude of the required control thrust remains limited. The low level of thrust would suggest the use of FEEP engines, which would lead to a minimal propellant consumption even over long operation times.

6 Acknowledgments

This research is partially supported by the ESA/Ariadna Study Grant AO/1-5387/07/NL/CB. The author would like to thank the reviewers for contributing to the improvement of this article.

References

[1] C. Colombo, M. Vasile, Optimal trajectories for NEO deflection, in: Proceedings of the 58th International Astronautical Congress, IAC-07-C1.4.02, Hyderabad, India, 2007.

[2] W. Hu, D. J. Scheeres, Spacecraft motion about slowly rotating asteroids, Journal of Guidance, Control and Dynamics 25 (4) (2002) 765–775.

[3] R. Kahle, E. Kuhrt, G. Hahn, J. Knollenberg, Physical limits of solar collectors in deflecting earth-threatening asteroids, Aerospace Science and Technology 10 (2006) 256–263.

[4] D. Lunan, Need we protect earth from space objects and if so, how?, Space Policy 8 (1) (1992) 90–91.

[5] C. Maddock, J. P. Sanchez Cuartielles, M. Vasile, G. Radice, Comparison of single and multi-spacecraft configurations for NEA deflection by solar sublimation, in: AIP Conference Proceedings 886: New Trends in Astrodynamics and Applications III, Princeton, USA, 2007, pp. 303–316.

[6] C. Maddock, M. Vasile, Design of optimal spacecraft-asteroid formation through a hybrid global optimization approach, International Journal of Intelligent Computing and Cybernetics 1 (2) (2008) 239–268.

[7] C. McInnes, Non-keplerian orbits for mars solar reflectors, Journal of the British Interplanetary Society 75 (2002) 74–84.

[8] H. J. Melosh, I. V. Nemchinov, Solar asteroid diversion, Nature 366 (366) (1993) 21–22.

[9] A. Rossi, F. Marzari, P. Farinella, Orbital evolution around irregular bodies, Earth Planets Space 51 (1999) 1173–1180.

[10] J. P. Sanchez Cuartielles, C. Colombo, M. Vasile, G. Radice, A multi-criteria assessment of deflection methods for dangerous NEOs, in: AIP Conference Proceedings 886: New Trends in Astrodynamics and Applications III, Princeton, USA, 2007, pp. 317–333.

[11] J. P. Sanchez Cuartielles, C. Colombo, M. Vasile, G. Radice, Multi-criteria comparison among several mitigation strategies for dangerous near earth objects, Journal of Guidance, Control and Dynamics to appear.

[12] H. Schaub, J. L. Junkins, Analytical Mechanics of Space Systems, AIAA Education Series, Virginia, USA, 2003.

[13] M. Vasile, Hybrid Behavioral-Based Multiobjective Space Trajectory Optimization, Studies in Computational Intelligence, Springer, 2008.

[14] M. Vasile, C. Colombo, Optimal impact strategies for asteroid deflection, Journal of Guidance, Control and Dynamics 31 (4) (2008) 858–872.